

**Lateral resistance of polyurethane-reinforced ballast with the application of new bonding schemes**

**Laboratory tests and discrete element simulations**

Jing, Guoqing; Zhang, Xu; Jia, Wenli

**DOI**

[10.1016/j.conbuildmat.2019.06.114](https://doi.org/10.1016/j.conbuildmat.2019.06.114)

**Publication date**

2019

**Document Version**

Accepted author manuscript

**Published in**

Construction and Building Materials

**Citation (APA)**

Jing, G., Zhang, X., & Jia, W. (2019). Lateral resistance of polyurethane-reinforced ballast with the application of new bonding schemes: Laboratory tests and discrete element simulations. *Construction and Building Materials*, 221, 627-636. <https://doi.org/10.1016/j.conbuildmat.2019.06.114>

**Important note**

To cite this publication, please use the final published version (if applicable).  
Please check the document version above.

**Copyright**

Other than for strictly personal use, it is not permitted to download, forward or distribute the text or part of it, without the consent of the author(s) and/or copyright holder(s), unless the work is under an open content license such as Creative Commons.

**Takedown policy**

Please contact us and provide details if you believe this document breaches copyrights.  
We will remove access to the work immediately and investigate your claim.

1 **Lateral resistance of polyurethane-reinforced ballast with the**  
2 **application of new bonding schemes: laboratory tests and discrete**  
3 **element simulations**

4  
5 Guoqing Jing<sup>a</sup>, Xu Zhang<sup>b,\*</sup> & Wenli Jia<sup>c</sup>  
6

7 <sup>a</sup> School of Civil Engineering, Beijing Jiaotong University, Beijing 100044, China

8 <sup>b</sup> School of Civil and Transportation Engineering, Guangdong University of Technology, Guangzhou 510006,  
9 China

10 <sup>c</sup> Faculty of Civil Engineering and Geosciences, Delft University of Technology, Delft, 2628CN, Netherlands

11

12 \* Corresponding author, e-mail: xuzhang@gdut.edu.cn

13

14 **Abstract:** To mitigate the ballast flight risk in the high-speed railway, this paper presents three new polyurethane  
15 bonding schemes which have negligible influence to tamping operations. With the application of these bonding  
16 schemes, a series of laboratory tests indicated that the polyurethane-reinforced ballast exhibited much larger  
17 lateral resistance than the ordinary ballast by 31% at least. Discrete element simulation results further  
18 demonstrated that the polyurethane improved the load-bearing capacity of the ballast at the particle scale through  
19 effectively restraining the particle movement. Therefore, the proposed bonding schemes ensure adequate lateral  
20 ballast resistance and are effective measures for improving the ballast performance.

21

22 **Key words:** high-speed railway; ballast; polyurethane; discrete element method; lateral resistance; single sleeper  
23 pull-out test

24

## 25 **1. Introduction**

26 Railway ballast is often constructed using crushed stones and works as an important granular layer  
27 under the track superstructure. One of the main functions of the ballast layer is to provide sufficient  
28 lateral resistance to the track panel so that the track geometry and stability can be kept and the train  
29 running safety can be ensured. Insufficient lateral ballast resistance may lead to some  
30 serious problems such as excessive movement of the track panel and track lateral buckling [1]. In  
31 order to provide enough lateral ballast resistance to the track, numerous measures have been taken  
32 all over the world to reinforce the ballast especially since the extensive application of the  
33 continuously welded rail (CWR) track which requires large lateral ballast resistance to prevent  
34 the track from bulking [2-6]. Among these measures, increasing the height of the shoulder  
35 ballast to be 100-150 mm over the ballast surface is considered as an effective way in China and  
36 many other countries for years.

37        However, with the rapid development of the high-speed railways over the past few years, the  
38 high shoulder ballast brings a new problem. It was reported that the shoulder ballast stones may fly  
39 due to the strong wind caused by the high-speed trains, and this phenomenon becomes a severe  
40 problem in the railways whose design speed reaches or exceeds 350 km/h [7,8]. Except for the  
41 shoulder ballast, the surface ballast stones near the sleeper centre also may fly easily due to the  
42 strong negative air pressure formed under the high-speed train bogies [7,9]. The ballast stones  
43 blowing up from the track during the train passage would probably strike the train components and  
44 the rail heavily which further results in failure or damage problems to the train and the rail [10].  
45 From the perspective of mitigating the ballast flight due to the high speed running of the trains, the  
46 height of the shoulder ballast should be decreased just as the flat ballast shoulder adopted in  
47 European railways. But regarding that the shoulder and crib ballast play important roles in the  
48 lateral ballast resistance [11], decreasing the height of the shoulder ballast will reduce the lateral  
49 ballast resistance to some extent though it is indeed helpful in mitigating the ballast flight. When the  
50 shoulder ballast height is decreased, other measures should be taken to gain enough lateral ballast  
51 resistance.

52        Aiming at this issue, the polyurethane, a kind of polymer material, has been applied to reinforce  
53 the ballast in recent years by bonding the granular ballast particles as a massive structure. To  
54 investigate the mechanical properties and performance of the polyurethane-reinforced ballast, a few  
55 laboratory and field tests have been conducted by researchers. According to the triaxial test results,  
56 Lee et al. [12] figured out that both the shear strength and the elastic moduli of the  
57 polyurethane-mixed ballast increase linearly with the content of the polyurethane. Woodward et al.  
58 [13-15] and Kennedy et al. [16] reported laboratory tests and engineering practices to show the  
59 applications of the polyurethane to help maintain track geometry and absolute clearances, to

60 improve the ballast stiffness and to reduce the ballast settlement. Woodward et al. [17] and  
61 Kruglikov et al. [18] presented that the lateral resistance of the ballast increased remarkably after  
62 the shoulder ballast was reinforced with the polyurethane along the longitudinal direction to form a  
63 block wall at the track side. Thomas et al. [19] demonstrated an application of the polyurethane to  
64 obtain more uniform load distribution of the ballasted track on a masonry bridge. These studies  
65 demonstrate that the polyurethane has been successfully applied to reinforce the railway ballast for  
66 many different goals. The relevant test results and engineering practices indicate that the application  
67 of the polyurethane really improves the ballast performance effectively.

68 Focusing on mitigating the ballast flight risk in high-speed railways, the polyurethane is often  
69 sprayed across the whole ballast surface. Fig. 1 illustrates the sketch of the widely adopted bonding  
70 scheme. Since all the particles from the surface to a certain depth in the ballast layer are strongly  
71 bonded by the polyurethane, this bonding scheme is effective in avoiding the ballast flight even in  
72 the cases when the trains run at very high speeds. However, this bonding scheme has an obvious  
73 disadvantage of affecting the tamping operations significantly. Because when all the surface ballast  
74 particles are entirely bonded with the polyurethane, it is quite difficult to insert the arms of the  
75 tamping machines into the bonded ballast to a required depth. New bonding schemes that can avoid  
76 the ballast flight and have negligible influence to the tamping operations simultaneously are very  
77 desirable for reinforcing the ballast in the high-speed railways. Meanwhile, although lots of studies  
78 have proved that it is effective to reinforce the ballast with the polyurethane, the mechanisms that  
79 how the polyurethane affects the micro-mechanical behaviours of the ballast have not been revealed  
80 yet, which still needs further insightful research.

## 81 **2 New bonding schemes for reinforcing the ballast with polyurethane**

82 This paper proposes three new bonding schemes, denoted as E, C & B, respectively, for reinforcing

83 the high-speed railway ballast with the polyurethane. In these new bonding schemes, only the  
84 ballast in four target regions instead of all the surface ballast are required to be bonded with the  
85 polyurethane. Fig. 2 demonstrates the four target regions where the ballast shall be bonded. Among  
86 these regions, two are at the sleeper ends and the other two are near the sleeper centre. In the  
87 proposed bonding scheme E, the shoulder ballast near the two sleeper ends are required to be  
88 bonded. In the bonding scheme C, the crib ballast near the sleeper centre shall be bonded, and in the  
89 bonding scheme B, both the ballast in the sleeper end and centre areas are required to be bonded.

90 | Since the target regions in Fig. 2 almost cover all the dangerous areas where the ballast flight is  
91 likely to occur, the new bonding schemes meet the requirement of avoiding the ballast flight by  
92 bonding the particles in these dangerous regions with the polyurethane. In the meantime, the new  
93 bonding schemes do not require the application of the polyurethane to the ballast in the areas near  
94 the rails where the tamping machines always work. Hence, the new bonding schemes have  
95 negligible influence to the tamping operations to the ballast. It is also worthy being noted that as  
96 indicated by the dimensions in Fig. 2, the target bonding regions in the three new bonding schemes  
97 are just 18.1%, 7.2%, and 25.3%, respectively, of the whole ballast surface, which can help reduce  
98 the dosage of the polyurethane distinctly. Also, with the new bonding schemes, the height of the  
99 ballast shoulder can be decreased, which reduces the dosage of the ballast material. Therefore,  
100 relative to the conventional bonding scheme, the new bonding schemes are more economical in the  
101 dosage of the ballast and the polyurethane material. In a word, the proposed bonding schemes  
102 simultaneously have multiple advantages of avoiding the ballast flight, reducing the dosage of the  
103 polyurethane and having negligible influence to the tamping operation.

104 However, the new bonding schemes have much smaller bonding area than the conventional  
105 scheme, and the ballast shoulder height is cancelled, both of which bring about a problem that

106 whether the lateral resistance of the ballast locally reinforced with the polyurethane based on the  
107 new bonding schemes is enough to keep the track lateral stability or not? Aiming at this issue,  
108 laboratory tests and discrete element simulations were carried out in this paper to investigate the  
109 lateral resistance of the ballast locally reinforced with the polyurethane based on the proposed  
110 bonding schemes. Two different bonding depth of 200 mm and 300 mm in the ballast were studied  
111 in the tests to investigate the feasibility of the new bonding schemes in providing enough lateral  
112 resistance for the high-speed railway track. Furthermore, the discrete element method (DEM) was  
113 employed in this paper to study the micro-mechanical behaviours of the ballast reinforced with the  
114 polyurethane since the DEM has the advantage in simulating the mechanical behaviours of granular  
115 materials. The mechanism that how the polyurethane materials helps increase the lateral ballast  
116 resistance was also studied and revealed through the DEM analyses.

### 117 **3 Laboratory tests on the lateral resistance of polyurethane-reinforced ballast**

118 The single sleeper pull-out test (SSPT) is an effective and frequently used method to evaluate the  
119 ballast resistance. In order to evaluate the lateral resistance of the ballast locally reinforced with the  
120 polyurethane, a series of laboratory tests were carried out using a full-scale test track and will be  
121 presented in this section.

#### 122 ***3.1 Material properties of ballast and polyurethane***

123 The ballast material adopted in the test is basalt with the particle size gradation illustrated in Fig.  
124 3, which meets the requirement of the ballast gradation standard in China. The polyurethane  
125 material utilized in this test was jointly developed by Beijing Jiaotong University and State Key  
126 Laboratory of Special Functional Waterproof Materials (SKLSFWM) in China. The polyurethane  
127 was produced by mixing two components, namely the component A-isocyanate & the component

128 B-polyols, with the volume ratio of 1:1. The strength of the produced polyurethane rapidly reaches  
129 70% of its final strength one day after the mixing and continues to increase with the time. The  
130 mechanical parameters of the polyurethane were measured in SKLSFWM and listed in Table 1.

### 131 **3.2 Test facility**

132 A full-scale test track comprising of sleepers and ballast was established in Beijing Jiaotong  
133 University. The total length of the test track was 12 m. The thickness of the ballast under the sleeper  
134 was 350 mm and the total width of the ballast bed was 3,600 mm. The width of the ballast shoulder  
135 was 500 mm and the slope was 1:1.75. The dimensions of the test track were consistent with those  
136 in the high-speed railway ballasted track in China.

137 The construction procedures of the test track are described hereinafter. Firstly, the ballast  
138 material were compacted in four layers with an electronic plate compactor to form the dense ballast  
139 bed. Then, the type IIIc pre-stressed concrete sleepers, which are frequently adopted for the  
140 ballasted track in China's high-speed railways, were laid on top of the ballast with the spacing of  
141 600 mm. After that, extra ballast material was put between the adjacent sleepers and at the sleeper  
142 ends, and compacted in three layers to form the crib and shoulder ballast. Finally, the polyurethane  
143 was sprayed from the top surface of the ballast using a specialized spray gun. The polyurethane then  
144 went down into the ballast to form coating on the surface of the ballast particles and bond the  
145 particles at the contacts.

146 Fig. 4 shows the photographs of the test track with and without the reinforcement of the  
147 polyurethane. For each of the three proposed bonding schemes, two test tracks with different  
148 bonding depth in the ballast, i.e. 200 mm and 300 mm, were constructed by controlling the dosage  
149 of the polyurethane material. As a reference, two extra test tracks were constructed without the  
150 reinforcement of the polyurethane. The summary of the laboratory tests that were carried out is



151 listed in Table 2. Among all the eight tests, the shoulder ballast height was only set in the test ‘Ns’,  
152 which represents the typical ballasted track in China with the shoulder ballast height of 150 mm. By  
153 comparing the results in the tests ‘Ns’ and ‘Nf’ that were carried out on the unreinforced ballast, the  
154 effect of the shoulder ballast height on the lateral resistance can be studied. For the other six tests,  
155 the first capital letters in their test names indicate the bonding scheme as discussed in Section 2 and  
156 the numbers after the capital letters indicate the bonding depth is 200 or 300 mm.

### 157 ***3.3 Test apparatus and procedures***

158 A set of specialized apparatus consisting of an oil pump, a force transducer, a reaction frame,  
159 two dial indicators and a data logger was developed and adopted to measure the lateral resistance  
160 force of the ballast and the lateral displacement of the sleeper in the SSPT. Fig. 5 presents the  
161 apparatus utilized for the measurement in the test.

162 In order to pull out the sleeper, the oil pump together with the force transducer and the reaction  
163 frame was horizontally installed at one sleeper end. The dial indicators were fixed above the sleeper  
164 with their pointers parallel to the sleeper. In the test, the oil pump was controlled to apply  
165 multi-stage loads to the sleeper. When the sleeper moved slowly under the horizontal load, the  
166 lateral force measured by the force transducer and the lateral displacement measured by the dial  
167 indicators were collected and saved in the data logger. Each load stage continued until the sleeper  
168 displacement increased to a stable value, and then the next stage of load was applied. Each test did  
169 not stop until the state that the lateral resistance force of the ballast almost kept stable. After each  
170 sleeper pull-out test, the test track including the ballast was dismantled and re-established with the  
171 same method as described in Section 3.2 for the next test, which ensured close ballast densities in  
172 all tests. Moreover, three repetitive tests were carried out for each test condition in Table 2. The  
173 measured results of the three tests were averaged as the test result for that load condition, and will

174 be presented in the paper.

### 175 **3.4 Test results**

176 Fig. 6 illustrates the lateral resistance force  $F$  of the reinforced ballast as a function of the lateral  
177 sleeper displacement  $d$  for the three new bonding schemes. In each subplot, the results of the tests  
178 ‘Ns’ and ‘Nf’ are also presented for comparison. It can be found the resistance force increases  
179 rapidly with the lateral sleeper displacement at the initial stage, and then gradually becomes stable  
180 when the sleeper displacement continues to increase. The lateral resistance force in the test ‘Ns’ is  
181 distinctly larger than that in the test ‘Nf’, which demonstrates the important contribution of the 150  
182 mm shoulder height to the lateral ballast resistance.

183 It also can be seen that the lateral resistance forces of the reinforced ballast based on all the  
184 three bonding schemes are remarkably larger than those in the tests ‘Ns’ and ‘Nf’. For the same  
185 bonding scheme, the larger lateral resistance force was gained for the reinforced ballast with the  
186 deeper bonding depth of 300 mm. These results indicate the application of polyurethane does result  
187 in distinct increase to the lateral ballast resistance. Furthermore, the deeper the ballast is bonded  
188 with the polyurethane, the larger is the lateral resistance of the reinforced ballast, which can be even  
189 larger than that of the unreinforced ballast with the shoulder height of 150 mm.

190 The lateral resistance force at the sleeper displacement of 2 mm obtained in the single sleeper  
191 pull-out test is always used for the quantitative evaluation of the lateral ballast resistance in  
192 practical engineering. To further quantify the lateral ballast resistance in the tests, the resistance  
193 forces at  $d=2$  mm were collected from the measured results in Fig. 6 and listed in Table 3. The  
194 relative differences between the lateral resistance forces of the reinforced ballast and those in the  
195 tests ‘Ns’ and ‘Nf’ were also calculated and listed in the table. It can be found when the sleeper  
196 displacement reached 2 mm, the resistance forces of the ballast were 10.02 kN and 7.05 kN,

197 respectively, in the tests ‘Ns’ and ‘Nf’. Apparently, without the ballast shoulder height, the lateral  
198 resistance force of the ballast decreases by nearly 30%.

199 When the ballast particles near the sleeper ends were bonded with the polyurethane, the lateral  
200 resistance force of the reinforced ballast with the bonding depth of 200 mm in the test ‘E2’  
201 increased by 41% relative to the test ‘Ns’ and by 60% relative to the test ‘Nf’. With the deeper  
202 bonding depth of 300 mm in the test ‘E3’, the lateral resistance force increased by 100% relative to  
203 the test ‘Ns’, and by 128% relative to the test ‘Nf’.

204 When the ballast near the sleeper centre was reinforced with the polyurethane with the bonding  
205 depth of 200 mm, the increase of the ballast lateral resistance force in the test ‘C2’ was 41% in  
206 contrast to that in the test ‘Ns’ and was 60% comparing with that in the test ‘Nf’. With the deeper  
207 bonding depth of 300 mm in the test ‘C3’, the lateral resistance force increased by 41% relative to  
208 that in the test ‘Ns’, and by 100% relative to that the test ‘Nf’.

209 When both the ballast near the sleeper ends and the sleeper centre were simultaneously  
210 reinforced with the bonding depth of 200 mm, the lateral resistance force in the test ‘B2’ increased  
211 by 70% with respect to the test ‘Ns’ and by 142% with respect to the test ‘Nf’. When the bonding  
212 depth was 300 mm, the ballast resistance in the test ‘B3’ increased by 100% with respect to the test  
213 ‘Ns’ and by 184% with respect to the test ‘Nf’.

214 Obviously, the lateral resistance force increased by 31% at least in the tests when the ballast was  
215 reinforced with the polyurethane with the application of the three new bonding schemes. The lateral  
216 resistance force of the reinforced ballast in the test ‘C2’ with the bonding depth of 200 mm was the  
217 minimum, which was 13.09 kN. But it was still larger than the specified minimum value of 12 kN  
218 for the ballast in China’s high-speed railways with the design speed higher than 250 km/h [20]. It  
219 means the lateral ballast resistances based on all the three new bonding schemes are adequate to

220 prevent the track from buckling.

221 Among the three bonding schemes, the maximum increment of the lateral resistance force was  
222 observed when the ballast was reinforced at both areas near the sleeper ends and its centre due to  
223 the largest bonding area in that case. In addition, comparing with the tests in which the bonding  
224 depth was 200 mm, the lateral resistance force of the reinforced ballast with the bonding depth of  
225 300 mm was larger by 14% when the ballast near the sleeper ends was reinforced, by 8% when the  
226 ballast near the sleeper centre was reinforced and by 17% when the ballast at both areas was  
227 reinforced. It can be concluded that the larger area and the larger thickness of ballast is reinforced  
228 with the polyurethane, the larger lateral ballast resistance can be gained.

#### 229 **4 Discrete element simulations on the lateral resistance of** 230 **polyurethane-reinforced ballast**

231 The DEM is a numerical method that excels in simulating the mechanical behaviours of the  
232 granular material. It was firstly developed by Cundall and Strack [21] and has been successfully  
233 applied to simulate the mechanical behaviours of railway ballast [22-27]. With the DEM, the  
234 contact forces between granular particles and the particle movement can be simulated, which is  
235 really helpful to investigate the micro-mechanical behaviours of the granular material.

236 The laboratory tests have shown distinct increase of the ballast resistance force when the ballast  
237 is reinforced with the polyurethane. In order to reveal the micro mechanism that how the  
238 polyurethane helps improve the lateral ballast resistance, the commercial DEM software Particle  
239 Flow Code (PFC) was employed in this paper to simulate the SSPTs. The PFC deals with the  
240 contact forces between particles based on the classic contact laws, and it calculates particle  
241 movement according to Newton's Second Law [28]. It also provides bond models to simulate the  
242 bonding behaviour between discrete particles, which can be used to simulate the bonding effect of

243 the polyurethane to the ballast particles. The DEM models that simulate the laboratory test track  
244 including the polyurethane-reinforced ballast and the simulation results on the SSPTs will be  
245 presented and discussed in this section.

#### 246 *4.1 Discrete element modelling of ballast particles and polyurethane*

247 The ballast particles always have irregular shapes and angular corners since they are stones  
248 mechanically crushed from intact rock. With the irregular shapes, the ballast particles interlock with  
249 each other to keep the ballast stability after they are compacted in the track. To simulate the contact  
250 and interlock behaviour between ballast particles well, discrete elements that can capture the  
251 realistic ballast particle shapes are desirable for the DEM modelling. In this research, rigid clumps  
252 with realistic particle shapes were generated with the laser scanning technique and the multi-sphere  
253 overlapping algorithm to simulate the ballast particles. Similar methods can be found in Refs.  
254 [26,29].

255 The procedures for generating the clumps are described here. First of all, three-dimensional  
256 images of real ballast particles were obtained using a handheld laser scanner-FreeScan X3, as  
257 shown in Fig. 7. Then, the images were imported into PFC to illustrate the particle surface, and the  
258 volume enclosed by each particle surface was completely filled with several overlapping spheres.  
259 Lastly, the irregular particle shape was approximated using a sufficient number of spheres with  
260 different diameters, and these overlapping spheres were regarded as a clump in the DEM simulation.  
261 In the present study, 20 real ballast particles with different shapes and size were scanned. Fig. 8  
262 presents the different particle shapes and the corresponding clumps generated in PFC. The number  
263 of the spheres composing each clump are also presented in the figure. Since there are a large  
264 number of ballast particles in the test track, these clumps were repeatedly used for the DEM  
265 modelling.

266 Utilizing the clumps, the contact behaviours between ballast particles were simulated with the  
267 linear contact model which allowed sliding between the contacting clumps. Besides, in order to  
268 simulate the ballast reinforced with the polyurethane, the bonding effects that the polyurethane  
269 provided to the ballast particles were modelled by creating parallel bonds at the particle contact  
270 points. When loading, these bonds can generate bond forces and moments to restrict the relative  
271 movements of the contacting particles. The bond forces and moments were linearly determined by  
272 the bond stiffness, the bond area and the particle relative movements according to the linear parallel  
273 bond (LPB) model which was implemented in PFC. The details of the LPB model can be found in  
274 the PFC manual [28]. Furthermore, the polyurethane material has a finite strength after enough  
275 curing time and it may fracture when the reinforced ballast subjects to large external load. The  
276 fracture behaviour of the polyurethane was also modelled with the LPB model. It means the parallel  
277 bond breaks when the normal or shear stress on the bond induced by the bond forces and moments  
278 exceeds the specified strength.

#### 279 *4.2 Discrete element simulations of SSPTs on ballast reinforced with polyurethane*

280 To simulate the SSPTs conducted in the laboratory, a 3D DEM model, as illustrated in Fig. 9a,  
281 was firstly established to simulate the sleeper and the ballast in the test track without any  
282 reinforcement. For the type IIIc sleeper, a stereo lithography (STL) file of the sleeper geometry was  
283 generated in the software AutoCAD and imported into PFC. Then wall elements were generated to  
284 reproduce the sleeper geometry. For the ballast, 45,355 clumps were generated according to the  
285 particle size distribution of the ballast in laboratory tests and compacted to achieve a desirable  
286 density. The side and base boundaries of the model were simulated using rigid wall elements. The  
287 dimensions of the DEM model were consistent with the test track except that only one sleeper bay  
288 was modelled here to reduce the simulation time while the laboratory test track has a total length of

289 12 m. In addition, after the DEM model was established, the sleeper was controlled to move down  
290 according to the numerical servo mechanism in PFC<sup>3D</sup> until the total vertical reaction force applied  
291 to the sleeper base reached 2.7 kN which was equivalent to the weight of a real sleeper.

292 Based on this DEM model, parallel bonds were created to further simulate the ballast reinforced  
293 with the polyurethane. Since not all the ballast particles were bonded with the polyurethane in the  
294 laboratory tests, the parallel bonds were only created at the contacts between the ballast particles  
295 that were located in the specified bonding region and depth according to each bonding scheme.  
296 Thus, the DEM models in which the ballast particles in specified areas were bonded with the  
297 parallel bonds were established to simulate the test tracks reinforced with the polyurethane to the  
298 depth of 200 mm, as illustrated in Fig. 9.

299 The main parameters in the DEM models were listed in Table 4. The contact stiffness of the  
300 particle-sleeper contacts were set much larger than that of the particle-particle contacts. It should be  
301 pointed out that in the laboratory tests, the polyurethane material was manually sprayed from the  
302 ballast top surface and automatically went down to the ballast voids due to its fluidity. Based on this  
303 fact, it can be inferred that the bond effects of the polyurethane were uniform in the whole ballast  
304 layer. Given the inhomogeneity of the bonding effects in the test track, the parallel bond stiffness  
305 and strength in the DEM model were assumed to follow the Gaussian distribution. The mean value  
306 of the normal bond strength was determined according the tensile strength of the polyurethane listed  
307 in Table 1. For various bonding schemes, the same values of the micro-mechanical parameters were  
308 used in the DEM models while the parallel bonds were created in different regions.

309 After the DEM models were established and cycled to equilibrium states, the simulations of the  
310 SSPTs were performed by moving the sleeper along the lateral track direction at a speed of 4 mm/s.  
311 This speed was set to be larger than that in the laboratory tests to save the computational time, and

312 the damping coefficient in the model was set to 0.5 to eliminate the dynamic effect due to the large  
313 moving speed. The maximum lateral displacement was set to 3 mm because the laboratory test  
314 results showed that the lateral resistance forces of the reinforced ballast were almost stable when the  
315 lateral displacement exceeded 3 mm. During the simulations, the lateral displacement of the sleeper  
316 and the lateral resistance force which was the lateral component of the sum of the contact forces  
317 between the sleeper and ballast particles were monitored to investigate the lateral ballast resistance  
318 responses.

#### 319 *4.3 Validation of discrete element models*

320 Fig. 10 presents the simulation results of the lateral resistance force-displacement responses of  
321 the reinforced ballast under various bonding schemes using the DEM models. The laboratory test  
322 results were also presented in the figure for comparison. It can be seen that the DEM results have  
323 good agreement with the test results when the sleeper displacement exceeds 2 mm, but there are  
324 obvious differences between them in the initial phase. A possible reason for the difference is that the  
325 large sleeper moving speed in the DEM simulations may result into reasonable dynamic effect to  
326 the ballast which was not fully eliminated even though the global damping coefficient of 0.5 had  
327 been considered. Meanwhile, the bonding behaviour of the polyurethane is quite complicated and  
328 may have large variations under different conditions. Lacking of the knowledge on the micro  
329 mechanical behaviours of the polyurethane bonds, a simple LPB model was adopted in the DEM  
330 simulations. To better capture the responses in the initial phase, the particle contact behaviours and  
331 the local bonding effects that the polyurethane applied to the ballast should be further investigated  
332 in the future.

333 Overall, the DEM results exhibit similar increase trends and close stable values with the test  
334 results for all the four bonding cases. When the lateral sleeper displacement reaches 2 mm, the



335 ballast resistance forces in the DEM results are 7.27, 14.30, 13.24 and 17.16 kN, respectively, for  
336 the unreinforced ballast and that reinforced at the sleeper ends, centre and both areas. These values  
337 are quite close to those measured in the tests as listed in Table 3. Hence, the established DEM  
338 models for the unreinforced and reinforced ballast are reasonable and can reproduce the lateral  
339 resistance force-displacement responses with good accuracy.

#### 340 ***4.4 Micro-mechanical behaviour analysis***

341 In order to reveal the mechanism that how the polyurethane improves the ballast resistance, the  
342 micro-mechanical behaviours of the ballast in the SSPTs are discussed hereinafter. According to the  
343 DEM simulation results, the maximum particle displacement and distributions of the contact force  
344 chains in the reinforced ballast are compared with those in the ordinary ballast without  
345 reinforcement to show the restraints that the polyurethane provides to the ballast at the particle  
346 scale.

347 Fig. 11 illustrates the force chain distributions in the ballast from different view angles when the  
348 lateral sleeper displacement reaches 3 mm. In this figure, solid lines are plotted at the particle  
349 contact points to represent the contact forces between ballast particles and those between the ballast  
350 and the sleepers. Each line is orientated along the direction of the contact force it represents and its  
351 thickness is proportional to the force magnitude. It can be observed that large contact forces are  
352 generated near the sleeper end and diffused to the shoulder ballast to provide resistance to the  
353 sleeper movement in all the four cases. For the ballasted track without the polyurethane, the  
354 maximum contact force between the ballast and the sleeper end is 650 N. When the polyurethane is  
355 applied to reinforce the ballast near the sleeper ends, near the sleeper centre and at both areas,  
356 respectively, the maximum contact force increases to 1235.7 N, 976.4 N and 1561.9 N. The  
357 maximum contact force increases by 90.1%, 50.2% and 1.4 times, respectively.

358 According to the DEM results, for the ballasted track without the polyurethane, the maximum  
359 particle displacement is 3.13 mm when the lateral sleeper displacement  $d$  reaches 3 mm. When the  
360 polyurethane is applied to reinforce the ballast near the sleeper ends, near the sleeper centre and at  
361 both regions, the maximum particle displacement decreases to 2.91 mm, 2.98 mm and 2.84 mm,  
362 respectively. The maximum particle displacement decreases by 7%, 4.8% and 9.3%, respectively.  
363 Apparently, the maximum particle displacement of the ballast was restrained to a certain degree due  
364 the bonding effect of the polyurethane to the ballast particles.

365 From the contact force chains and particle displacement results, it can be understood that the  
366 polyurethane successfully restrains the ballast particle movement and improves the load-bearing  
367 capacity of the granular ballast at the particle scale. This is because the polyurethane provides  
368 strong bonding effect to the ballast particles so that effectively restrains the particle movement  
369 induced by the squeezing and friction effect of the sleeper. With the large-area and effective  
370 bonding of the polyurethane, the granular ballast particles are integrated to form a more stable  
371 load-bearing structure. Hence, the polyurethane-reinforced ballast can provide larger resistance  
372 force to the sleeper by restraining the particle movement inside it and increasing the contact force  
373 network intensity.

## 374 **5 Conclusions**

375 This paper has proposed three new bonding schemes to reinforce the ballast with polyurethane more  
376 efficiently by merely bonding the ballast near the sleeper ends or centre, or in both areas. Whereas  
377 the shoulder ballast height is cancelled and the bonding area is small, the lateral resistance of the  
378 polyurethane-reinforced ballast with the application of the new bonding schemes were investigated  
379 in the paper.

380 A series of single sleeper pull-out tests were carried out to study the lateral resistance

381 force-displacement responses of the reinforced ballast. The test results indicated that if the ballast  
382 was reinforced with polyurethane based on the proposed bonding schemes, the ballast resistance  
383 was larger than that of the ordinary ballast without any reinforcement by at least 31%. These results  
384 demonstrate that all the three new bonding schemes can ensure adequate ballast lateral resistance to  
385 keep track stability.

386 Discrete element models were also established to simulate the SSPTs using clumps with realistic  
387 particle shapes. Parallel bonds were created in the models to simulate the bonding effect of the  
388 polyurethane to the ballast particles. The simulation results of the DEM models showed good  
389 agreement with the laboratory test results. According to the DEM results, the particle displacement  
390 and the contact force chains were analysed to investigate the micro-mechanical behaviours of the  
391 reinforced ballast. It was found that the bonding effect of the polyurethane at the particle scale can  
392 effectively restrain the movement of ballast particles and thereby successfully integrate the granular  
393 ballast to form a more stable load-bearing structure, which provides larger ballast resistance force to  
394 the sleeper than the ordinary granular ballast.

395 After the evaluation of ballast resistance in this study, the proposed bonding schemes have the  
396 advantages of mitigating the ballast flight, saving the dosage of the polyurethane, having negligible  
397 influence to the tamping operation and providing adequate ballast resistance simultaneously. These  
398 bonding schemes can be chosen by engineers to mitigate the ballast flight risk in the high-speed  
399 railways or to increase the ballast resistance effectively.

## 400 **Acknowledgements**

401 This work is supported by the Natural Science Foundation of China (NSFC) project under grant No. 51578051  
402 and the Guangdong University of Technology Youth Fund under grant 18QNZD002.

## 403 **References**

- 404 [1] Esveld, C. (2001). *Modern railway track*, second edition. MRT-productions, The Netherlands.
- 405 [2] Esmaeili, M., Khodaverdian, A., Neyestanaki, H. K., & Nazari, S. (2016). Investigating the effect of nailed  
406 sleepers, on increasing the lateral resistance of ballasted track. *Computers & Geotechnics*, 71, 1-11.
- 407 [3] Esmaeili, M., Zakeri, J. A., & Babaei, M. (2017). Laboratory and field investigation of the effect of  
408 geogrid-reinforced ballast on railway track lateral resistance. *Geotextiles & Geomembranes*, 45(2), 23-33.
- 409 [4] Kasraei, A., Zakeri, J. A., Esmaeili, M., & Bakhtiary, A. (2016). A numerical investigation on the lateral  
410 resistance of frictional sleepers in ballasted railway tracks. *Proceedings of the Institution of Mechanical  
411 Engineers, Part F: Journal of Rail & Rapid Transit*, 10(6), 1-10.
- 412 [5] Koike, Y., Nakamura, T., Hayano, K., & Momoya, Y. (2014). Numerical method for evaluating the lateral  
413 resistance of sleepers in ballasted tracks. *Soils & Foundations*, 54(3), 502-514.
- 414 [6] Tutumluer, E., Huang, H., Hashash, Y., and Ghaboussi, J. (2006). Aggregate shape effects on ballast tamping  
415 and railroad track lateral stability. *Proc., Annual Conf. of the American Railway Engineering and  
416 Maintenance-of-Way Association, American Railway Engineering and Maintenance-of-Way Association,  
417 Lanham, MD.*
- 418 [7] Quinn, A. D., Hayward, M., Baker, C. J., Schmid, F., Priest, J. A., & Powrie, W. (2010). A full-scale  
419 experimental and modelling study of ballast flight under high-speed trains. *Proceedings of the Institution of  
420 Mechanical Engineers, Part F: Journal of Rail & Rapid Transit*, 224(2), 61-74.
- 421 [8] Premoli, A., Rocchi, D., Schito, P., Somaschini, C., & Tomasini, G. (2015). Ballast flight under high-speed  
422 trains: wind tunnel full-scale experimental tests. *Journal of Wind Engineering & Industrial Aerodynamics*, 145,  
423 351-361.
- 424 [9] Jönsson, M., Ehrenfried, K., Loose, S., & Wagner, C. (2014). Particle image velocimetry of the underfloor  
425 flow of generic high-speed train models in a water towing tank. *Proceedings of the Institution of Mechanical  
426 Engineers, Part F: Journal of Rail & Rapid Transit*, 228(2), 194-209.

- 427 [10] Goo, J. S., Kim, J. S., & Shin, K. B. (2015). Evaluation of structural integrity after ballast-flying impact  
428 damage of a grip lightweight bogie frame for railway vehicles. *Journal of Mechanical Science & Technology*,  
429 29(6), 2349-2356.
- 430 [11] Le Pen, L., & Powrie, W. (2011). Contribution of base, crib, and shoulder ballast to the lateral sliding  
431 resistance of railway track: a geotechnical perspective. *Proceedings of the Institution of Mechanical Engineers*,  
432 Part F: *Journal of Rail & Rapid Transit*, 225(2), 113-128.
- 433 [12] Lee S. H., Lee, S. J., Park, J. G., & Choi, Y. T. (2017). An experimental study on the characteristics of  
434 polyurethane-mixed coarse aggregates by large-scale triaxial test. *Construction & Building Materials*, 145,  
435 117-125.
- 436 [13] Woodward, P. K., Kacimi, A. E., Laghrouche, O., Medero, G., & Banimahd, M. (2012). Application of  
437 polyurethane geocomposites to help maintain track geometry for high-speed ballasted railway tracks. *Journal*  
438 *of Zhejiang University-Science A (Applied Physics & Engineering)*, 13(11), 836-849.
- 439 [14] Woodward, P. K., Kennedy, J., Medero, G. M., & Banimahd, M. (2012). Maintaining absolute clearances in  
440 ballasted railway tracks using in situ three-dimensional polyurethane geocomposites. *Proceedings of the*  
441 *Institution of Mechanical Engineers, Part F: Journal of Rail & Rapid Transit*, 226(226), 257-271.
- 442 [15] Woodward, P. K., Kennedy, J., Laghrouche, O., Connolly, D. P., & Medero, G. (2014). Study of railway track  
443 stiffness modification by polyurethane reinforcement of the ballast. *Transportation Geotechnics*, 1(4),  
444 214-224.
- 445 [16] Kennedy, J., Woodward, P. K., Medero, G., & Banimahd, M. (2013). Reducing railway track settlement using  
446 three-dimensional polyurethane polymer reinforcement of the ballast. *Construction & Building Materials*,  
447 44(3), 615-625.
- 448 [17] Woodward, P. K., Kennedy, J., Medero, G. M., & Banimahd, M. (2012). Application of in situ polyurethane  
449 geocomposite beams to improve the passive shoulder resistance of railway track. *Proceedings of the*

- 450 Institution of Mechanical Engineers, Part F: Journal of Rail & Rapid Transit, 226(3), 294-304.
- 451 [18] Kruglikov, A. A. Yavna, V. A. & Ermolov, Y. M. (2017). Strengthening of the railway ballast section shoulder  
452 with two-component polymeric binders. *Transportation Geotechnics*, 11: 133-143.
- 453 [19] Thomas, S., Woodward, P., & Laghrouche, O. (2015). Influence of stiffening ballasted track bed overlying a  
454 masonry arch bridge using a polyurethane polymer material. *Construction & Building Materials*, 92, 111-117.
- 455 [20] National Railway Administration of P.R. China. (2014). Code for design of high speed railways. China  
456 Railway Press, Beijing. (in Chinese)
- 457 [21] Cundall, P. A., & Strack, O. D. L. (1979). A discrete numerical model for granular assemblies. *Geotechnique*,  
458 29(30), 331-336.
- 459 [22] Chen, C., Mcdowell, G. R., and Thom, N. H. (2012). Discrete element modelling of cyclic loads of  
460 geogrid-reinforced ballast under confined and unconfined conditions. *Geotextiles and Geomembranes*,  
461 35(35):76-86.
- 462 [23] Indraratna, B., Ngo, N. T., Rujikiatkamjorn, C., and Vinod, J. S. (2012). Behaviour of fresh and fouled  
463 railway ballast subjected to direct shear testing: discrete element simulation. *International Journal of*  
464 *Geomechanics*, 14(1):34-44.
- 465 [24] Tutumluer, E., Qian, Y., Hashash, Y. M. A., Ghaboussi, J., and Davis, D. D. (2013). Discrete element  
466 modelling of ballasted track deformation behaviour. *International Journal of Rail Transportation*, 1(1-2):57-73.
- 467 [25] Zhang, X., Zhao, C., & Zhai, W. (2017). Dynamic behavior analysis of high-speed railway ballast under  
468 moving vehicle loads using discrete element method. *International Journal of Geomechanics*, 17(7):  
469 04016157.
- 470 [26] Zhang X., Zhao C. & Zhai W. (2019). Importance of load frequency in applying cyclic loads to investigate  
471 ballast deformation under high-speed train loads. *Soil Dynamics and Earthquake Engineering*, 120:28-38.
- 472 [27] Ling, X., Xiao, H., & Cui, X. (2018). Analysis of mechanical properties of polyurethane-mixed ballast based

- 473        on energy method. *Construction & Building Materials*, 182, 10-19.
- 474    [28] Itasca Consulting Group. (2008). *Particle flow code in three dimensions (PFC3D)*, Minneapolis.
- 475    [29] Anochie-Boateng, J. K., Komba, J. J., & Mvelase, G. M. (2013). Three-dimensional laser scanning technique
- 476        to quantify aggregate and ballast shape properties. *Construction & Building Materials*, 43(43), 389-398.

477 **Table list:**

478 Table 1 Mechanical properties of the polyurethane used in the test

Parameter	Value
Density (g/cm <sup>3</sup> )	1.13
Tensile strength (MPa)	14.2
Elongation at break (%)	20
Tearing strength (N/mm)	60
Shore hardness	46

479

480 Table 2 Summary of the tests carried out in the laboratory

Test name	Shoulder height (mm)	Bonding area	Bonding depth from the top surface (mm)
Ns	150	None	0
Nf	0	None	0
E2	0	At sleeper ends	200
E3	0	At sleeper ends	300
C2	0	near sleeper center	200
C3	0	near sleeper center	300
B2	0	both areas	200
B3	0	both areas	300

481



482

483

Table 3 Lateral resistance forces of ballast at  $d=2\text{mm}$  in various tests and their differences

Test	Lateral resistance force (kN)	Difference from Ns	Difference from Nf
Ns	10.0	-	42%
Nf	7.05	-30%	-
E2	14.09	41%	100%
E3	16.07	60%	128%
C2	13.09	31%	86%
C3	14.09	41%	100%
B2	17.08	70%	142%
B3	20.02	100%	184%

484

485

486

Table 4 The micro-mechanical parameters in the DEM simulations

Parameters	Value	Parameters	Mean value	Standard error
Damping coefficient	0.5	Parallel bonds		
Ballast particles		Normal stiffness ( $\text{N/m}^2$ )	$1.5 \times 10^7$	$1.0 \times 10^6$
Clump density ( $\text{kg/m}^3$ )	2700	Shear stiffness ( $\text{N/m}^2$ )	$1.5 \times 10^7$	$1.0 \times 10^6$
Normal stiffness ( $\text{N/m}$ )	$1 \times 10^8$	Tensile strength (Pa)	$1.42 \times 10^7$	$1.0 \times 10^6$
Shear stiffness ( $\text{N/m}$ )	$1 \times 10^8$	Cohesive strength (Pa)	$1.42 \times 10^7$	$1.0 \times 10^6$
Friction coefficient	0.5	Friction angle ( $^\circ$ )	45	0
Ballast-sleeper contacts				
Normal stiffness ( $\text{N/m}$ )	$5 \times 10^9$			
Shear stiffness ( $\text{N/m}$ )	$5 \times 10^9$			
Friction coefficient	0.5			

487

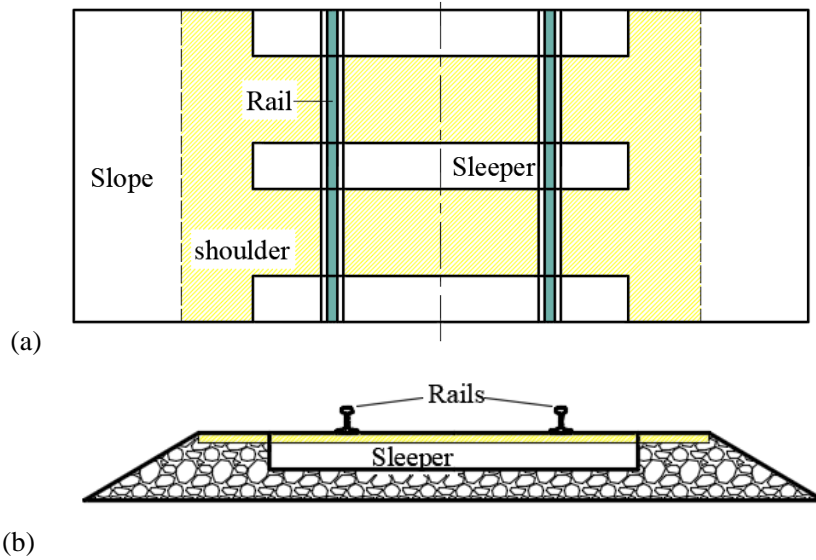


Fig. 1 Sketch of the target region (in yellow) in the conventional bonding scheme for reinforcing the ballast with polyurethane: (a) plane view and (b) end view

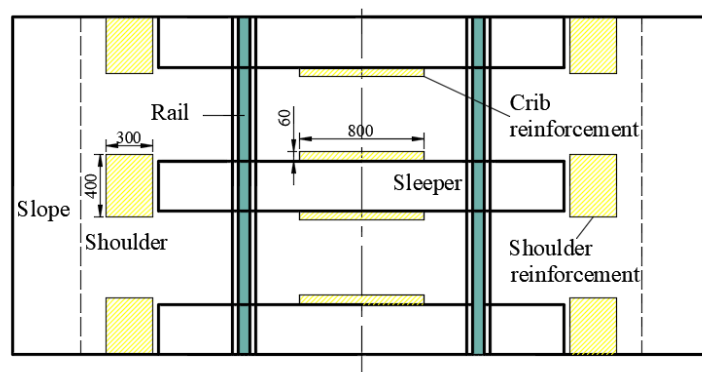


Fig. 2 Sketch of the target regions (in yellow) in the new bonding schemes for reinforcing the ballast with polyurethane (unit: mm)

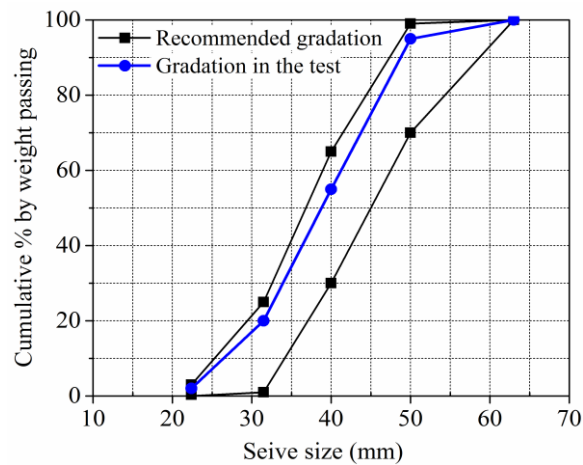


Fig. 3 Particle size gradation of ballast in the tests

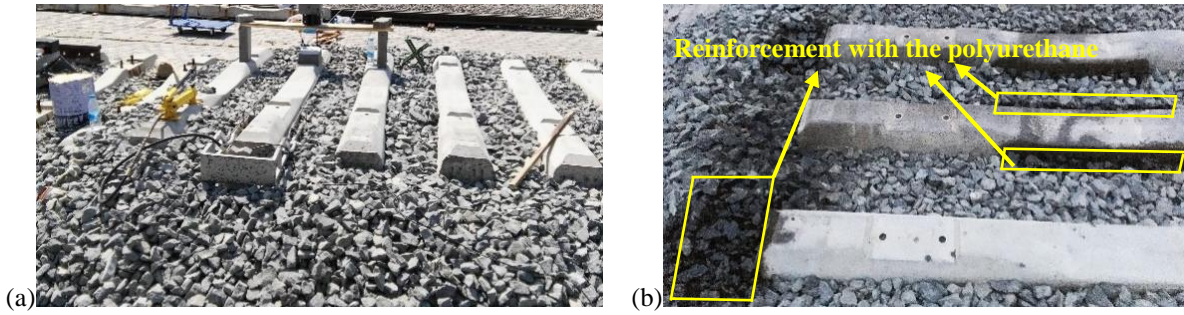


Fig. 4 Photographs of the ballasted track with and without the reinforcement of the polyurethane: (a) without reinforcement, (b) reinforced at both regions

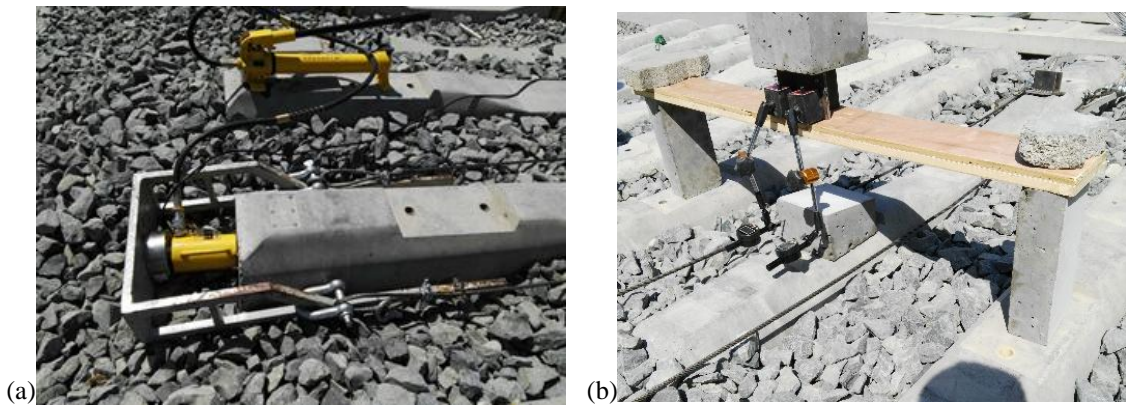


Fig. 5 Apparatus for measuring (a) the lateral resistance force of the ballast and (b) the lateral displacement of the sleeper

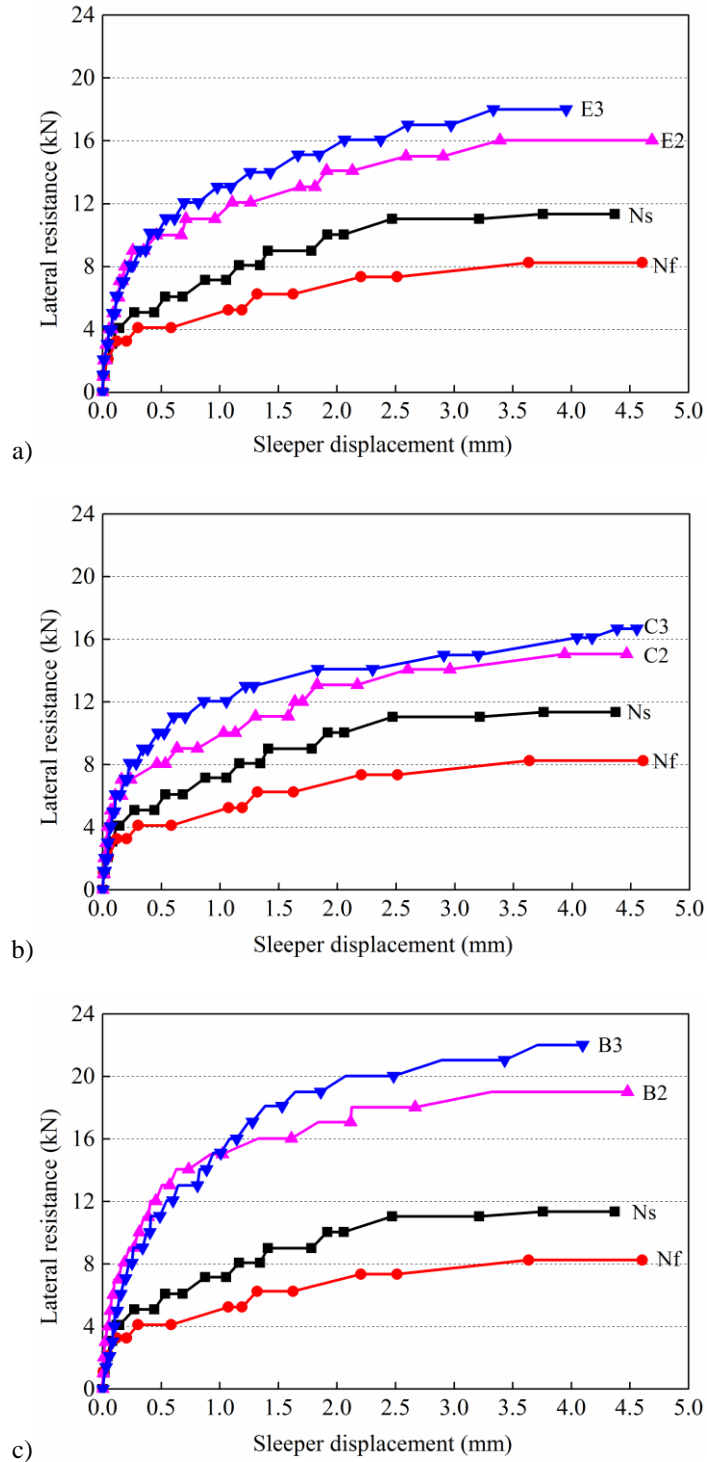


Fig. 6 Test results of the lateral resistance force-displacement responses of the reinforced ballast based on various bonding schemes: (a) reinforced near the sleeper ends, (b) reinforced near the sleeper centre and (c) reinforced at both regions

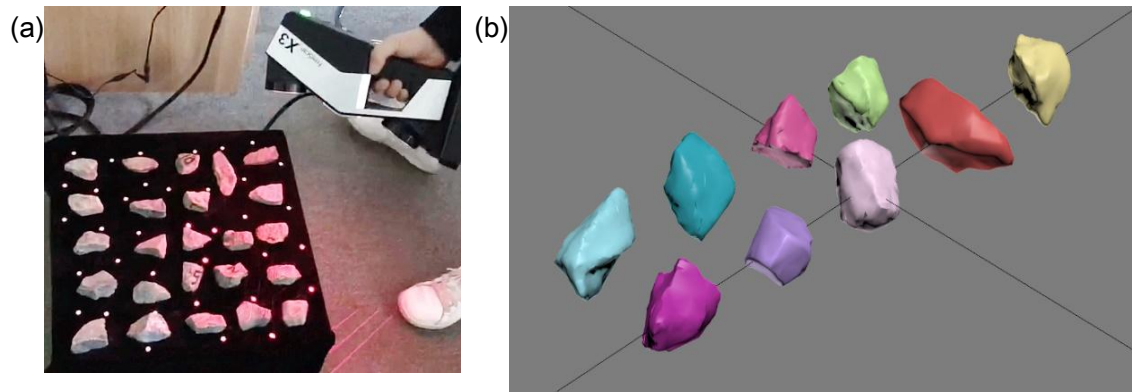


Fig. 7 3D laser scanning of ballast particles: (a) photograph of scanning and (b) the scanned images

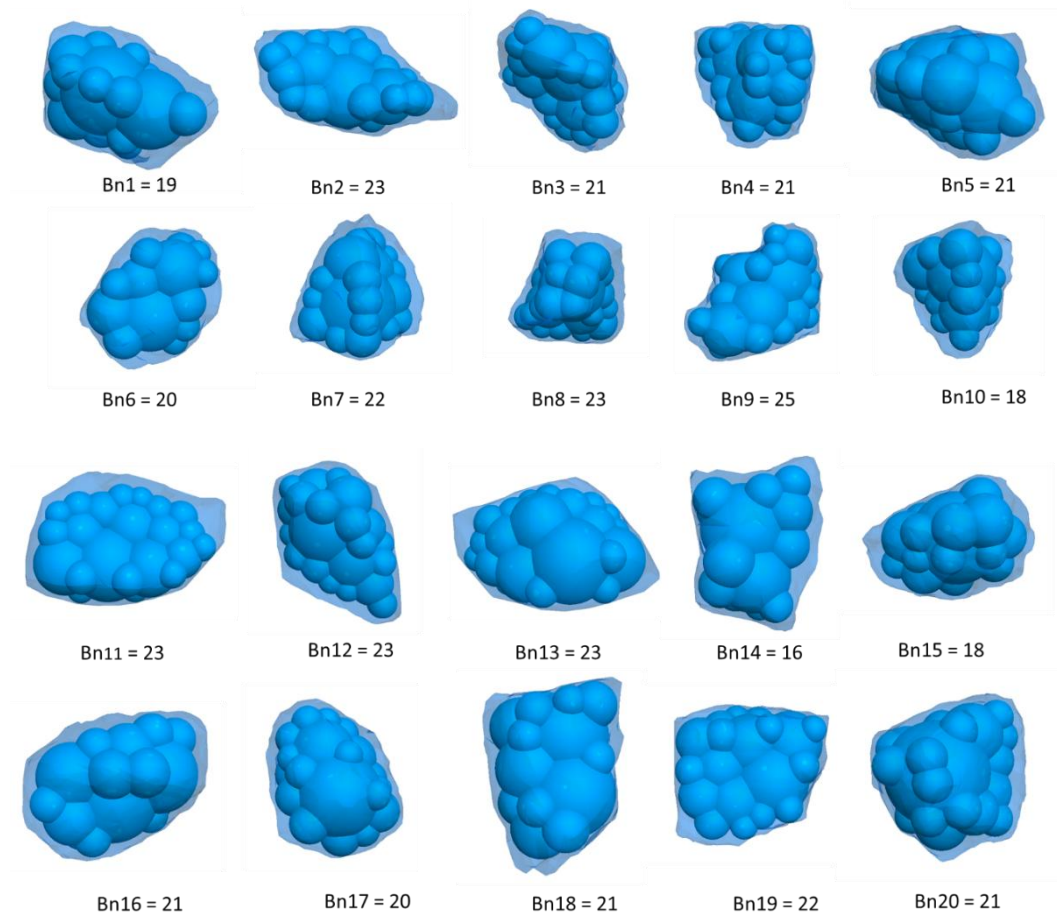


Fig. 8 Ballast particle shapes and clumps generated in PFC



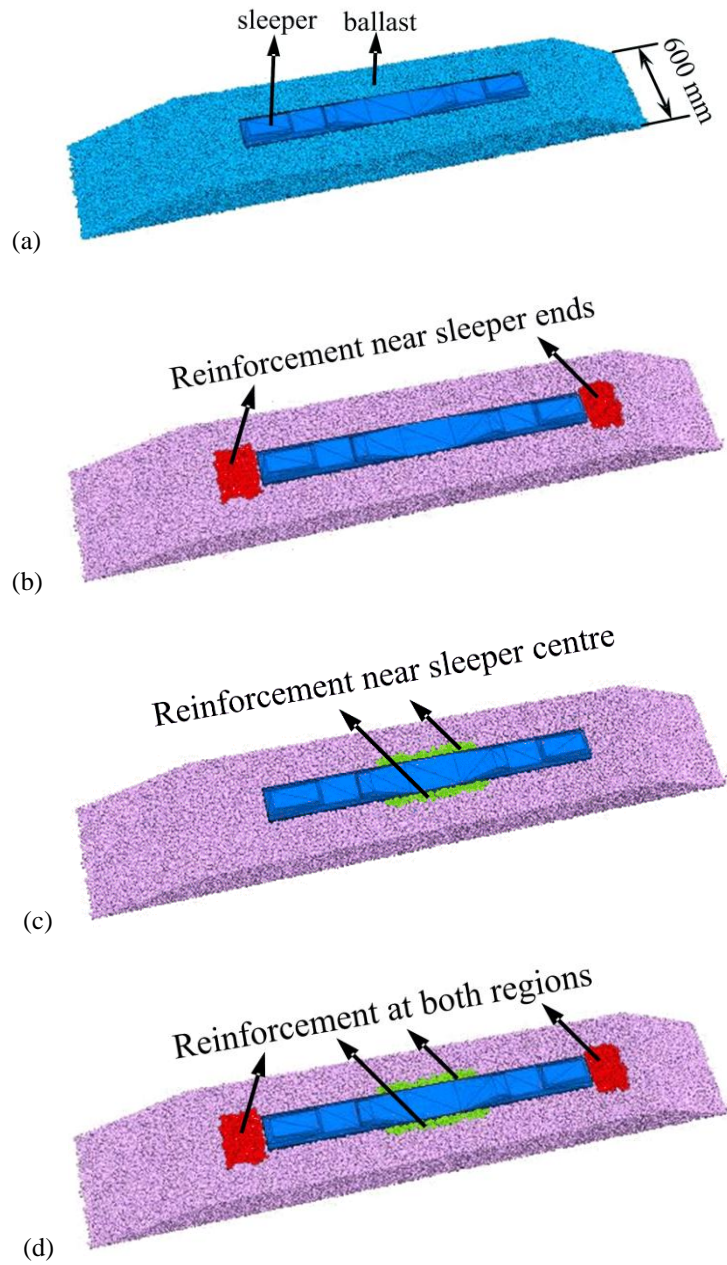


Fig. 9 The DEM models of the sleeper-ballast structure with and without the reinforcement of polyurethane: (a)without reinforcement, (b)reinforced near the sleeper ends, (c)reinforced near the sleeper centre and (d)reinforced at both regions

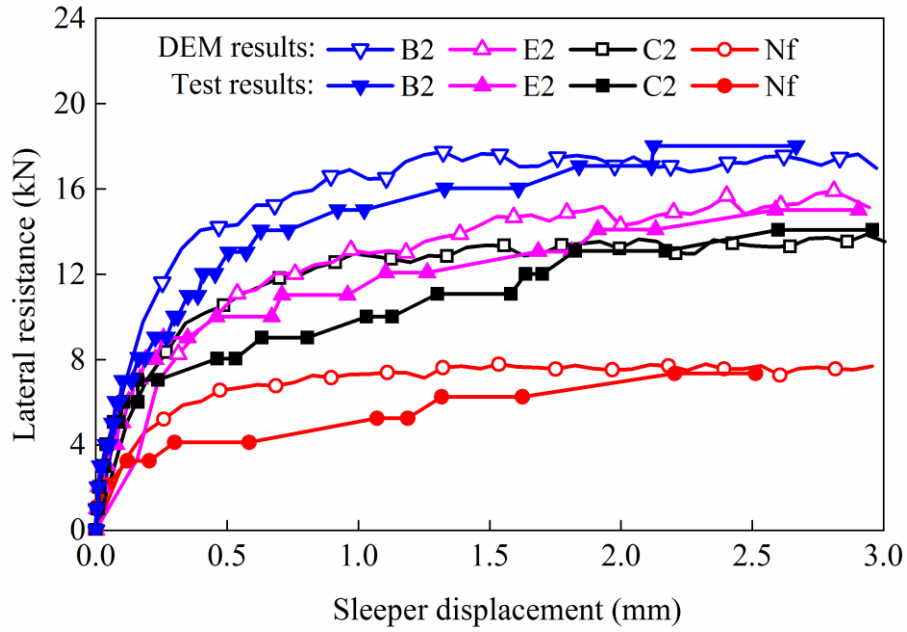


Fig.10 The resistance force-displacement responses of the reinforced ballast: a comparison between the DEM and test results

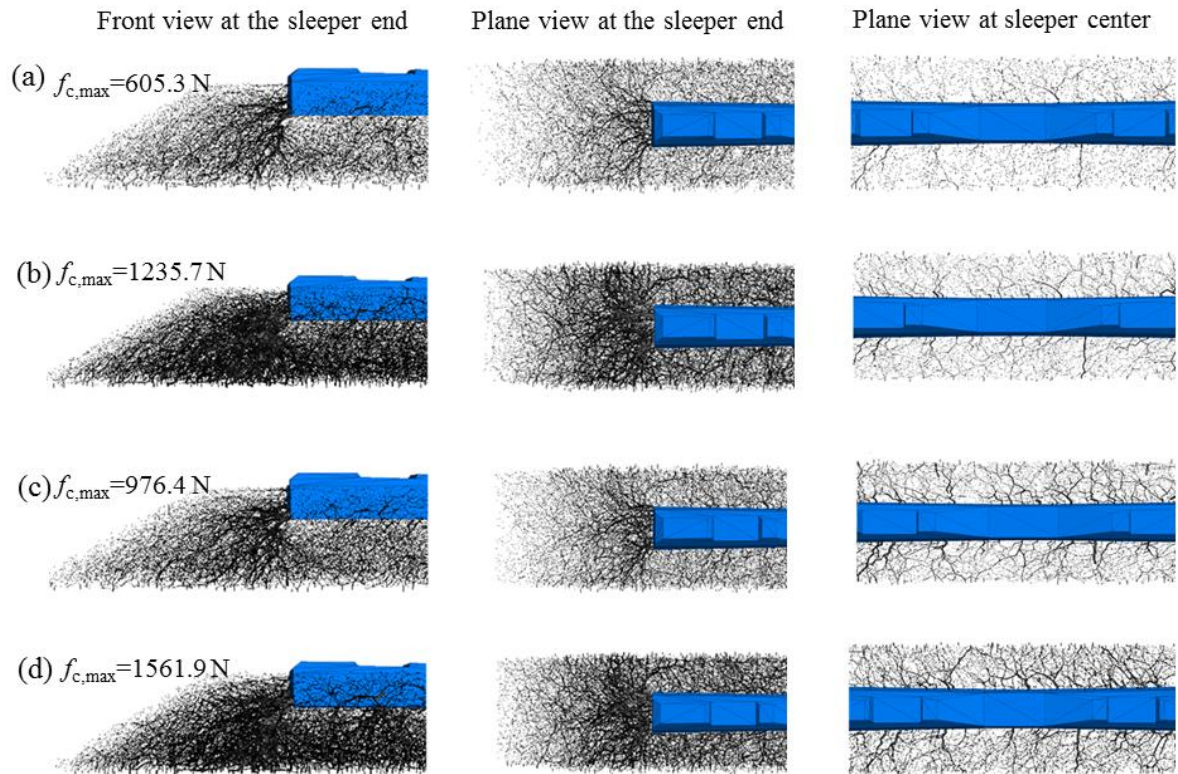


Fig.11 Contact force chains distributions in the ballast at  $d=3\text{mm}$ : (a) unreinforced ballast, (b) reinforced near the sleeper ends, (c) reinforced near the sleeper center and (d) reinforced at both regions